Agriculture, Ecosystems and Environment 269 (2019) 204–214

Contents lists available at ScienceDirect

Agriculture, Ecosystems and Environment

journal homepage: www.elsevier.com/locate/agee

Spatio-temporal dynamics of soil moisture driven by 'Grain for Green' program on the Loess Plateau, China

Luping Ye[a,b], Linchuan Fang[a], Zhihua Shi[a,c], Lei Deng[a], Wenfeng Tan[a,c,*]

[a] State Key Laboratory of Soil Erosion and Dryland Farming on the Loess Plateau, Institute of Soil and Water Conservation, Chinese Academy of Sciences and Ministry of Water Resources, Yangling 712100, China

[b] University of Chinese Academy of Sciences, Beijing 100049, China

[c] Key Laboratory of Arable Land Conservation (Middle and Lower Reaches of Yangtze River), Ministry of Agriculture, Huazhong Agricultural University, Wuhan 430070, China

ARTICLE INFO

Keywords:
Afforestation
Evapotranspiration
NDVI
Precipitation
Loess Plateau
Soil moisture

ABSTRACT

The continuous afforestation has led to significant changes in soil moisture (SM) dynamics on the Loess Plateau, China (LPC). However, evaluating the spatio-temporal distributions and driving factors of the SM changes following afforestation is challenging because of the difficulty of accessing areas and the lack of long-term series records. Here, we evaluated the accuracy of Global Land Evaporation Amsterdam Model (GLEAM) SM product by comparing with in-situ SM data in LPC, and quantified the spatio-temporal variations of SM in different periods from 1982 to 2015 under the 'Grain for Green' program (GGP). The results showed that the Normalized Difference Vegetation Index (NDVI) was well matched with the SM variations in more than 46% area of LPC from 1982 to 2015, which mainly located at the vegetated areas. The variations of SM responding to re-vegetation displayed obvious southeast-negative and northwest-positive patterns, which was the wet region (annual precipitation > 450 mm) to be dry and dry region (annual precipitation ≤450 mm) to be wet. Path coefficient value revealed that the positive effect of vegetation activity for grassland on SM was ascribed to its promotion on the occurrence of rainfall (mean path coefficient = 0.278). Precipitation played vital impact on the SM in bareland and sparsely vegetated area, and evapotranspiration played a dominant role in the SM dynamic of the forestland, especially at the early stage of GGP (From 2000 to 2010), while precipitation and NDVI had stronger effects than evapotranspiration on the SM dynamics of grassland. Our study suggests that in arid and semi-arid areas, vegetation achieves the optimal water retention capacity when the vegetation fractions are 1.4%–3.7% and 3.8%–7.2%, respectively. Hence, vegetation should not be further expanded in semi-humid areas, but should be further restored in arid and semi-arid areas with sparse or excessively sparse vegetation cover (especially in desert).

1. Introduction

Arid and semi-arid ecosystems (called hereafter "drylands") occupy 41% of global land surface and support over 38% of the world's population (Reynolds et al., 2007). Revegetation programs in drylands such as 'Grain for Green' Program (GGP) have been implemented extensively (Deng et al., 2016, 2017). They provide opportunities for promoting the ecosystem services, such as climate change regulation, carbon sequestration improvement, and soil water retention, etc (Piao et al., 2006; Yuan et al., 2016). Meanwhile, revegetation programs could have significantly impact on soil moisture (SM) changes, especially in the arid and semi-arid areas (Deng et al., 2016).

SM plays a vital role in hydrologic cycle and are greatly influenced by climatic factors (precipitation, temperature and evapotranspiration) (Lawrence and Vandecar, 2014), vegetation characteristics (plant species, age and density) (Deng et al., 2016; Manoli et al., 2016), soil properties with soil texture, soil porosity and soil organic matter, etc (Schlaepfer et al., 2017), topographic attributes, and land-use/land-cover patterns (Van Loon et al., 2016). Soil water mainly comes from the infiltration from precipitation or irrigation and the recharge from groundwater, and its reduction mainly by evaporation, root uptake, surface runoff, and infiltration to deeper soil layers. SM dynamic contributes to a variable but continuous spatial redistribution of soil water (Schlaepfer et al., 2017). SM is the most primary limiting factor for

* Corresponding author at: Key Laboratory of Arable Land Conservation (Middle and Lower Reaches of Yangtze River), Ministry of Agriculture, College of Resources and Environment, Huazhong Agricultural University, Wuhan 430070, China.
E-mail address: tanwf@mail.hzau.edu.cn (W. Tan).

https://doi.org/10.1016/j.agee.2018.10.006
Received 13 August 2018; Received in revised form 9 October 2018; Accepted 10 October 2018

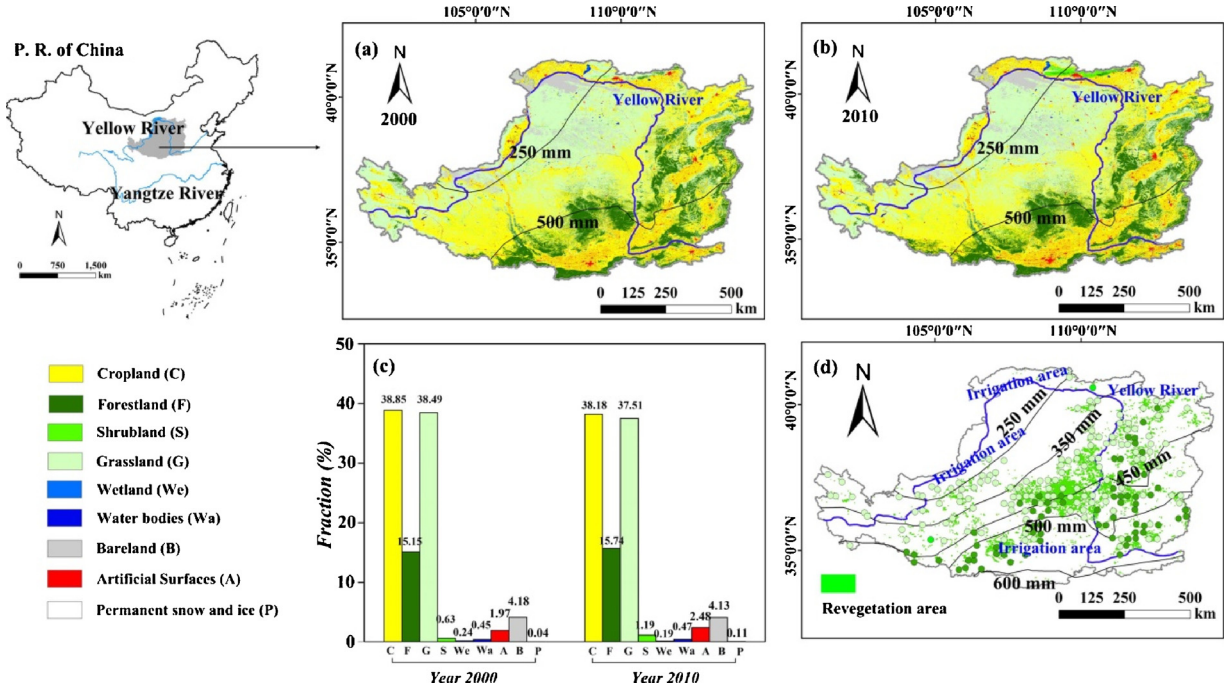

Fig. 1. Study area. Spatial distributions of land cover types over the Loess Plateau based on GLC2000 (the Global Land Cover 2000 Project) data: (a) Year 2000, (b) Year 2010; (c) The fraction of land use types in different years; (d) The distributions of revegetation area and rainfall zones.

drylands vegetation, and greatly impacts on the spatio-temporal distribution of vegetation (Feng et al., 2016), on the contrary, vegetation activity also plays a vital role in regulating SM dynamics, especially after extensive afforestation (Deng et al., 2016).

Vegetation cover affects SM by precipitation partitioning, such as canopy interception, throughfall and stemflow (McColl et al., 2017). The precipitation intercepted by plant canopies has no direct contributions to SM (Llorens and Domingo, 2007), while throughfall and stemflow have direct effects on the spatio-temporal variation of SM (Durocher, 1990). The satellite-derived vegetation indices such as Normalized Difference Vegetation Index (NDVI), which is widely used at local to global scale, was used to represent the vegetation activity (Jasechko et al., 2013; Ortiz et al., 2008; Peng et al., 2017). Revegetation dramatically decreases the SM by increasing evaporation, retaining precipitation on the leaves, and root water uptake (Li and Shao, 2006). A significant decline of SM has been reported in both deep and surface soil layers after planting of trees (Chen et al., 2008; Deng et al., 2016). However, SM is increased by the lower land surface temperature and soil evaporation under plant canopy shadows as well as by the higher rainfall infiltration into soil, canopy storage and collection in tree trunk (Jiao et al., 2016). Revegetation influences the exchange of energy and water between land surface and atmosphere, which affects precipitation occurrence (Piao et al., 2008). In general, the balance between soil water input and output is vital for understanding the water cycle in the terrestrial ecosystem, especially in arid and semi-arid ecosystems (Wang et al., 2008). Therefore, it is important to explore the response of SM dynamics to revegetation on drylands.

The Loess Plateau, China (LPC) is one of the most representative drylands ecosystems and eroded landscape in the world (Fu, 1989). Intensive agricultural practices had caused extremely severe soil erosion in the LPC. Thus, several practical measurements on soil and water loss control have been implemented since the 1980s to give information on optimizing the land use pattern and configuration, including the building of terraces and sediment-trapping dams, banning grazing and afforestation in bareland. But soil erosion was still severe in cultivated slope cropland. Then, GGP, one of the most well-known revegetation programs (Deng et al., 2012, 2017), has been implemented in the LPC to restore the fragile ecosystems by converting slope cropland ($> 25^{\circ}$) and bareland into grassland, shrubland and woodland since 1999 and expanded to the whole plateau in 2000 (Feng et al., 2016). The vegetation cover of the LPC has been almost doubled from 1999 to 2010 after the implementation of GGP (Chen et al., 2015b). The significant achievements of GGP in controlling soil erosion have been widely acknowledged (Deng et al., 2012), but there is a new confusion about whether revegetation positively or negatively affects SM dynamics.

Currently, the understanding of SM dynamics in drylands seems to be fragmented, since previous researches have been mainly focused on the impacts of vegetation activity, precipitation and evapotranspiration on SM at a short period of time (Yang et al., 2014; Zhang et al., 2009). At a transect scale, Yang et al. (2017) have proposed that SM dynamics are highly variable under different land use types. Although there have been some recent reports about the variations of SM under different land use types and in different rainfall zones in the LPC (Deng et al., 2016; Feng et al., 2016), very limited literatures focus on the impact of vegetation perturbation (such as returning farmland to forestland or grassland) on the spatio-temporal patterns of SM dynamics. In addition, the individual contribution of vegetation activity, evapotranspiration and precipitation to SM still remains poorly understood.

Over the past three decades, many efforts have been made to develop satellite SM products (Miralles et al., 2011; Park et al., 2017; Wang, 1985). Global Land Evaporation Amsterdam Model (GLEAM) SM product, which spans the period 1980–2016 with spatial resolution of $0.25^{\circ} \times 0.25^{\circ}$, assimilates microwave observations of SM from the European Space Agency's Climate Change Initiative (CCI-SM). It shows a general good agreement with in situ SM (Martens et al., 2016). GLEAM SM product provides opportunities to explore spatio-temporal dynamics of SM back to 1982, and thus to analyze its drives by revegetation. However, these opportunities have not been fully utilized, especially in drylands. Therefore, the specific objectives of this study are to: (1) evaluate the performance of GLEAM SM product in capturing the spatio-temporal dynamics of SM on the LPC; (2) obtain the spatio-temporal distributions of SM change trend across the LPC from 1982 to 2015; (3) determine whether and how vegetation cover, evapotranspiration and precipitation directly/indirectly affect SM dynamics, and (4) preliminarily assess the effects of GGP on SM.

2. Materials and methods

2.1. Study area

The LPC is located within 33.72°–41.27 °N, 100.90°–114.55 °E, and 200–3000 m altitude, with an area of approximately 6.4×10^5 km^2 (Fig. 1). The region is in an arid and semi-arid continental monsoon climate zone. The mean annual precipitation (MAP) is 420 mm and ranges from 150 mm in the northwest to 800 mm in the southeast, about 55%–78% of which concentrates in the wet season (Xin et al., 2011; Zhao et al., 2017). The period from July to September is defined as wet season and other months are regarded as dry season (Wang et al., 2017b). It is considered as one of the most seriously eroded landscapes in the world. As one of the most well-known revegetation program, GGP was started in 1999 and expanded in 2000s to the whole plateau (Zhou et al., 2012), with the greatest intensity in the first ten years. In addition, the impact of vegetation on SM tended to be more stable after 8–10 years of tree planting compared with in the early stage (Wang et al., 2011). According to the GlobeLand30 (http://www.globeLand30.org) (Chen et al., 2015a), which developed by National Geomatics Center of China (NGCC), the vegetations in LPC are classified into 4 types: Cropland (C), Forestland (F), Shrubland (S), and Grassland (G) (Fig. 1a, b).

2.2. Datasets

The data of root-zone (10–250 cm) and surface (0–10 cm) SM were retrieved from the Global Land Evaporation Amsterdam Model (GLEAM) Version 3.0a with a spatial resolution of 0.25° global grid. GLEAM aims at deriving the physical process of evapotranspiration by combining different satellite images. The land-cover type of each grid cell was classified as tall vegetation such as forestland (soil depth: 0–10, 10–100 and 100–250 cm), low vegetation such as grassland (soil depth: 0–10 and 10–100 cm) and bare soil (soil depth: 0–10 cm) (Martens et al., 2017). A detailed algorithm has been described by Miralles et al. (2011). According to the method of a previous study (Feng et al., 2017), the availability of GLEAM SM was validated by in-situ SM in the LPC, which the information in details was showed in Supporting Information (SI) (Fig. S1). And we assumed that there was a constant error and reliability for root-zone and surface data. GLEAM also provides the evapotranspiration data in 1982–2015. Given that the groundwater depth exceeds 250 cm, the supply of water by rainfall to groundwater was not taken into account (Li and Huang, 2008).

NDVI equals to the ratio of the difference to the sum in the reflectance of near-infrared band and red band. The NDVI data were obtained from Advanced Very High Resolution Radiometer (AVHRR) developed by the Global Inventory Modeling and Mapping Studies (GIMMS) group. The GIMMS NDVI dataset in 1982–2015 was derived at a spatial resolution of 1/12° and a temporal resolution of 15 days (https://ecocast.arc.nasa.gov/data/pub/gimms/3g.v1/). The datasets for monthly precipitation (1982–2015) were collected from Chinese Meteorological Data Network (http://data.cma.cn/). All data are resampled to 0.25° × 0.25°. Figs. S2–S4 display the spatial patterns of NDVI, evapotranspiration and precipitation. The meteorological station data were used to validate the rationality of resampled data (Fig. S5). Fig. S6 shows the changes of annual SM, NDVI, evapotranspiration and precipitation during the period of 1982–2015.

2.3. Statistical analyses

Based on each pixel point, the unary linear regression was used to determine the variation trends of SM in both root-zone and surface soil, NDVI, evapotranspiration, and precipitation. The formula is as follows (Mao et al., 2012):

$$b = \frac{n \times (\sum_{i=1}^{n} x_i y_i) - \left(\sum_{i=1}^{n} x_i\right) \times \left(\sum_{i=1}^{n} y_i\right)}{n \times \left(\sum_{i=1}^{n} x_i^2\right) - \left(\sum_{i=1}^{n} x_i\right)^2} \quad (1)$$

where b is the slope of the change trend, n is the number of observed years, x_i is the year serial number, y_i is the mean value of *SM*, *NDVI*, *evapotranspiration*, or *precipitation* in observed years. Positive and negative values of b indicate an increase and decrease of y, respectively.

The factors that affect SM are interrelated with each other in the geosystem. Hence, when studying the correlation of two factors in a multi-factor system, other factors should be excluded in a partial correlation analysis. To understand the impacts of NDVI, evapotranspiration and precipitation on SM dynamics, the partial correlation analysis between SM and one factor (e.g. NDVI) was performed after statistically controlling other factors (e.g. evapotranspiration and precipitation), using the formula as follows (Velicer, 1976):

$$r_{xy \times z} = \frac{r_{xy} - r_{xz} r_{yz}}{\sqrt{(1 - r_{xz}^2)(1 - r_{yz}^2)}} \quad (2)$$

where $r_{xy} = \frac{\sum (x - \bar{x})(y - \bar{y})}{\sqrt{\sum (x - \bar{x})^2 \sum (y - \bar{y})^2}}$.

where $r_{xy \times z}$ is the partial correlation coefficient between variable x and y, with controlling the effect of variable z, r_{xy}, r_{xz} and r_{yz} are correlation coefficients between variable x and variable y, variable x and variable z, and variable y and variable z, respectively.

F test and t-test were used to determine the significance of the change trend and partial correlation coefficient, respectively. Their equations were shown in SI text. The spatial distributions of NDVI, evapotranspiration and precipitation trends in the LPC and their significance levels are displayed in Figs. S7–S9 and S10, respectively. Lindeman-Merenda-Gold (LMG) method was used to further quantify the relative importance of NDVI, evapotranspiration and precipitation in determining the SM. It was performed in R software (version 3.4.3) with the package “relaimpo” (Gromping, 2006).

In order to analyze the effects of NDVI, evapotranspiration and precipitation on SM dynamics more clearly, the LPC was divided into three rainfall zones based on the standard classification criteria for arid and semi-arid areas: Rainfall zone I (< 250 mm, arid area), Rainfall zone II (250–500 mm, semi-arid area) and Rainfall zone III (> 500 mm, semi-humid area) (Huang et al., 2016). Based on the implementation intensity of GGP and the impact of vegetation on SM, four separate periods, including 1982–2015 (P0), 1982–1999 (P1, before GGP), 2000–2010 (P2, early stage of GGP), and 2011–2015 (P3, later stage of GGP), were selected to examine the spatio-temporal patterns of the chosen eco-environmental factors.

2.4. Path analysis

Before path analysis, the revegetation area was converted to 209 points to extract the data of SM in root-zone and surface soil, NDVI, evapotranspiration and precipitation from 1982 to 2015 (Fig. 1d). Based on land use types, these 209 points were divided into grassland and woodland (including forestland and shrubland). Then, partial correlation analysis was performed based on the extracted data. The dynamic changes of partial correlation coefficients of SM with NDVI, evapotranspiration and precipitation divided the period of 1982–2015 into four stages: 1982–1998 (before GGP), 1999 (beginning of GGP), 2000–2007 (early stage of GGP), and 2008–2015 (later stage of GGP) (Fig. S11). Path analysis presents the direct and indirect relationships between variables in a multivariate statistical analysis (Wang et al., 2017a). It partitions the correlation coefficients into components and shows as path coefficients. Here, we used path analysis to separate the direct and indirect effects of NDVI, evapotranspiration and precipitation on SM dynamics in grassland or woodland during different stages.

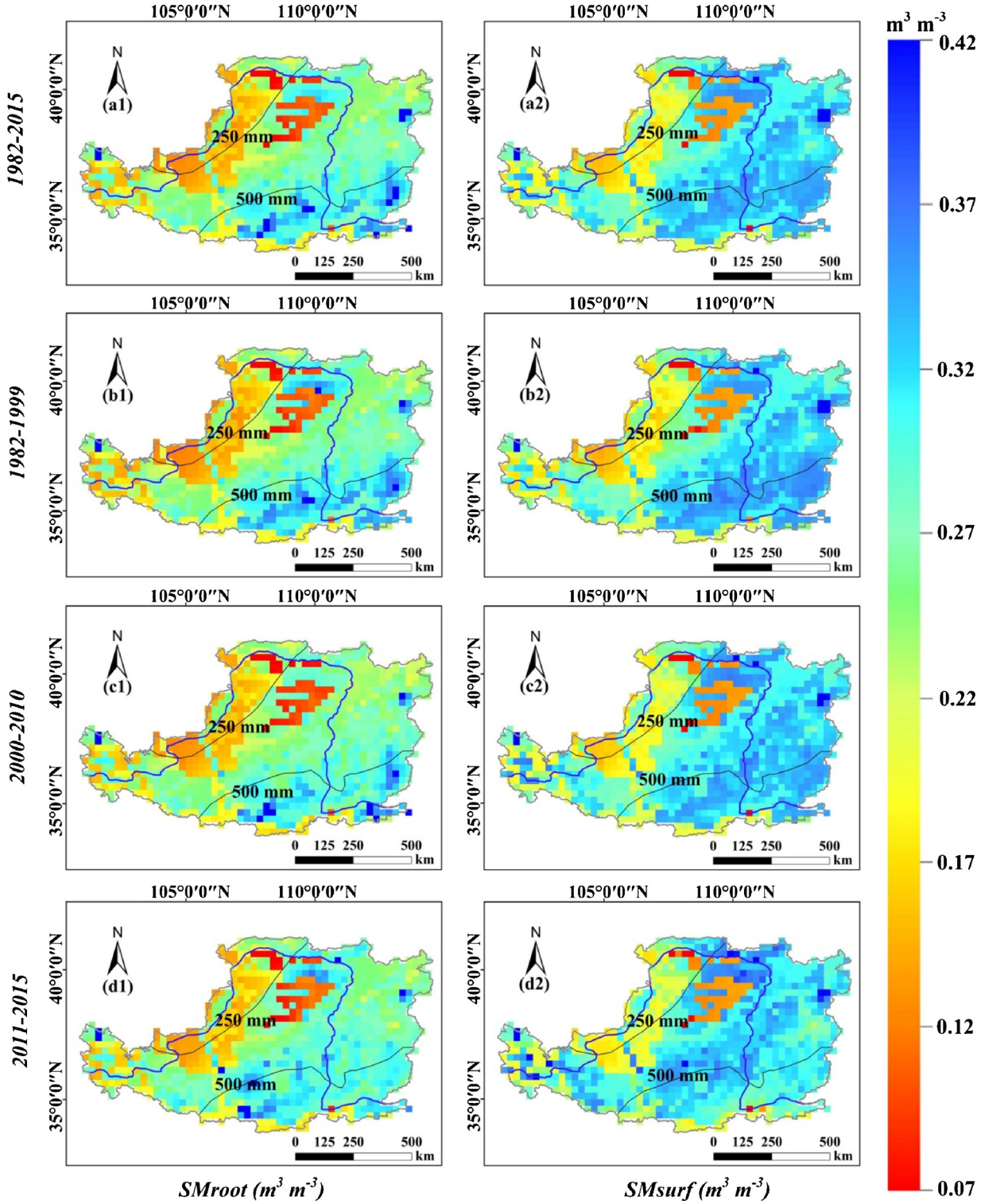

Fig. 2. Spatial distributions of annual mean soil moisture (SM) over the Loess Plateau during the four periods: 1982–2015 (first row), 1982–1999 (second row), 2000–2010 (third row) and 2011–2015 (fourth row). The SM distributions are estimated in root-zone (a1, b1 c1 and d1) and surface soil (a2, b2, c2 and d2), respectively. SMroot and SMsurf represent the soil moisture in root-zone and surface soil, respectively.

3. Results

3.1. Spatio-temporal pattern of soil moisture dynamic

There had an obvious gradient in annual SM climatology in both root-zone and surface soil from northwestern to southeastern LPC and Mu Us desert was the most arid area in the LPC (Fig. 2). SM was higher in surface soil compared with in root-zone soil. The validation of Global Land Evaporation Amsterdam Model (GLEAM) SM availability showed that the data range was 0.16 ± 0.06 $m^3 m^{-3}$ for in-situ SM, 0.07 ± 0.02 $m^3 m^{-3}$ for the Japanese Aerospace Exploration Agency (JAXA) SM, and 0.31 ± 0.03 $m^3 m^{-3}$ for GLEAM SM. However, the relationships between GLEAM SM and MODIS leaf area index (LAI)/ land surface temperature (LST) were consistent with those between in

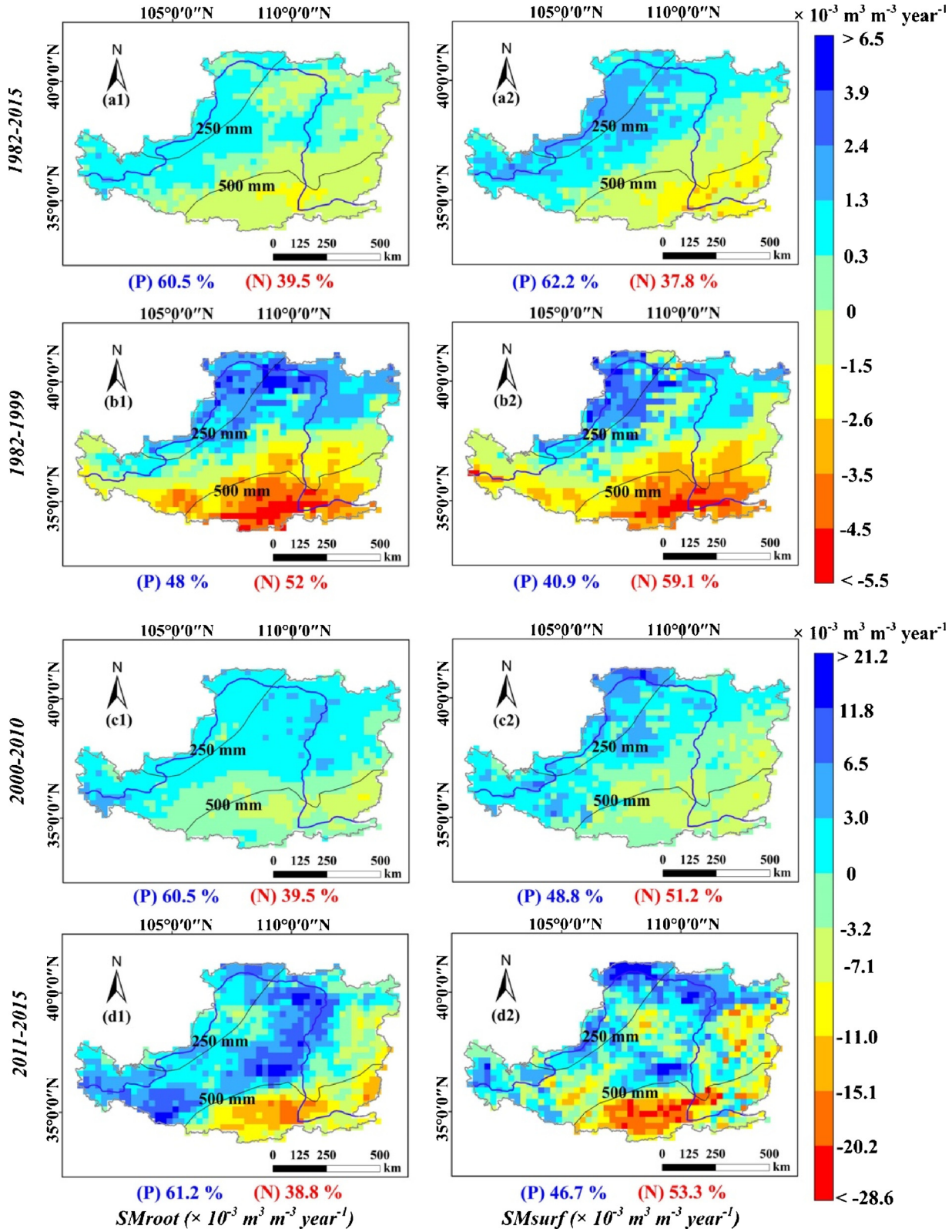

Fig. 3. Spatial distributions of annual trends in soil moisture over the Loess Plateau during the four periods: 1982–2015 (first row), 1982–1999 (second row), 2000–2010 (third row) and 2011–2015 (fourth row). The trends are estimated in root-zone (a1, b1 c1 and d1) and surface (a2, b2, c2 and d2), respectively. SMroot and SMsurf represent the soil moisture in root-zone and surface soil, respectively. P and N in the lower panel of maps represent the percentages of pixels displaying positive and negative trends, respectively.

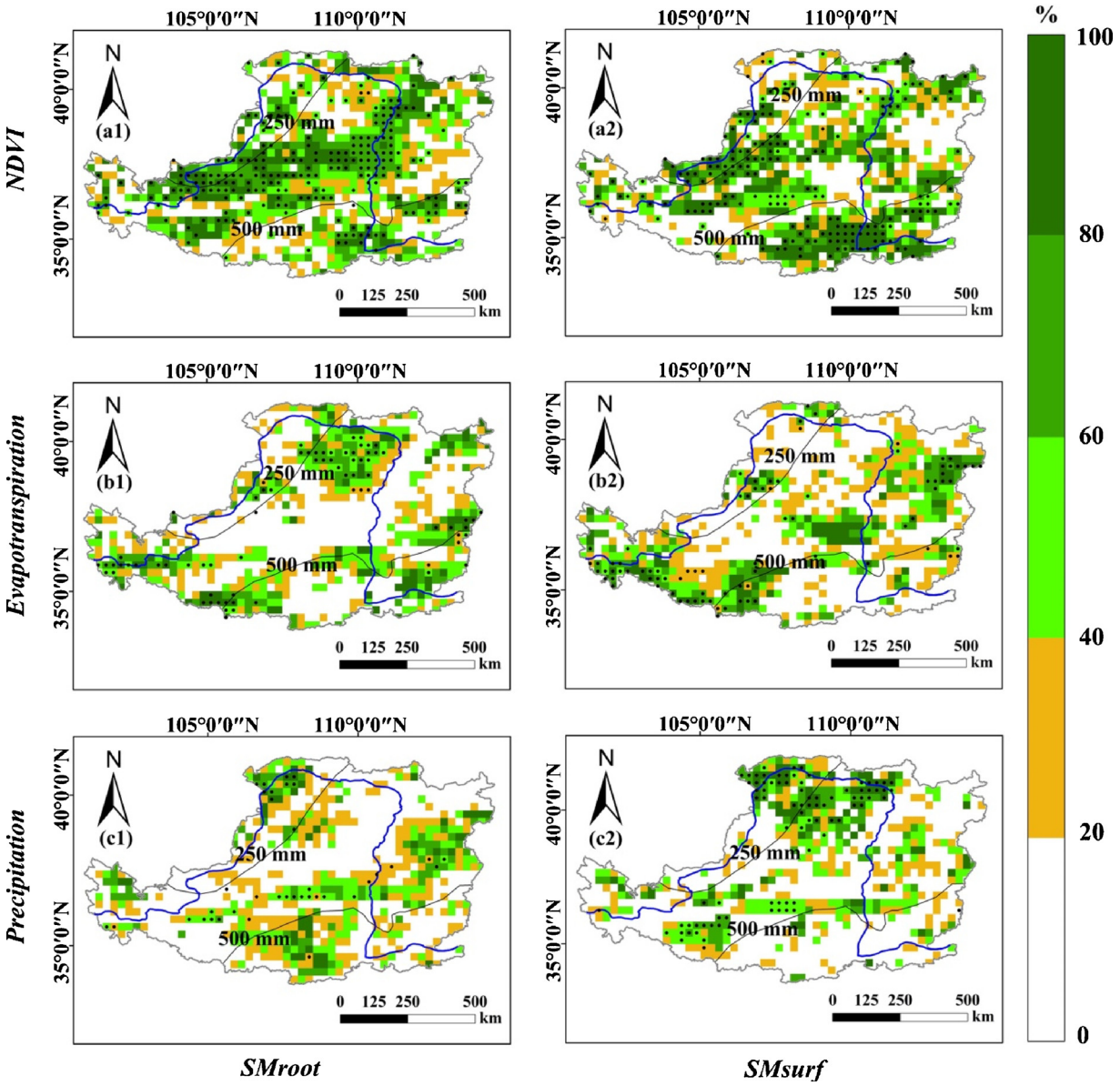

Fig. 4. NDVI, evapotranspiration, and precipitation drivers for soil moisture interannual variability. SMroot, SMsurf, and NDVI represent soil moisture in root zone, soil moisture in surface soil, and normalized difference vegetation index, respectively. Black points mark pixels with significant contribution to annual soil moisture (statistically significant at $P < 0.1$).

situ SM and MODIS LAI/LST (Fig. S1). These results suggested that GLEAM SM data had a same applicability for evaluating the spatio-temporal variations of SM in the LPC just as JAXA SM.

There had fluctuating trends for SM in both root-zone and surface soil in the LPC during 1982–2015 (Fig. S6). On the spatial scale, there was a widespread drying trend from 1982 to 2015 in Rainfall zone III, with an average rate of $-1.06 \pm 0.42 \times 10^{-3}\,m^3\,m^{-3}\,yr^{-1}$ in root-zone soil and $-1.42 \pm 0.75 \times 10^{-3}\,m^3\,m^{-3}\,yr^{-1}$ in surface soil, and 99% (29%, $P < 0.05$) and 98% (62%, $P < 0.05$) of the entire area show negative trends (Fig. S10 a1–a4 and b1–b4, Tables S1–S2), respectively. This drying trend during the period of P3 (2011–2015) was faster than that during the periods of P1 (1982–1999) and P2 (2000–2010). But for the arid area, there was a wetting trend during the four periods. In Rainfall zone II, the wetting trend spatially expands to the southeast side of the LPC from P1 to P2 and P3 (Fig. 3). In summary, the change trends of SM in different rainfall zones showed that the wetter area (MAP > 450 mm) tends to get drier while the drier area tends to get wetter from 1982 to 2015 throughout the LPC (Fig. 3, Fig. S6, and Tables S1–S2). SM in surface soil decreased more quickly than that in root-zone soil after the implementation of GGP.

3.2. Spatio-temporal patterns of NDVI, evapotranspiration and precipitation dynamics

The results showed green area in the LPC increased gradually from the arid area to the semi-humid area, which was in accordance with the spatial distribution of the implementation of GGP and the hydrothermal gradient in the LPC (Figs. 1d and S2, S4). There was an obvious increasing trend for the annual-mean GIMMS NDVI during 1982–2015, especially in the last decade. The spatial distributions of annual-mean evapotranspiration (Fig. S3) and precipitation (Fig. S4) also exhibited same regional characteristics. Compared with NDVI, evapotranspiration and precipitation had more fluctuant inter-annual variations throughout the LPC from 1982 to 2015 (Fig. S6).

The change trends of NDVI, evapotranspiration and precipitation were subsequently examined (Figs. S7–S9). Similar greening trends

were found in dry, wet season and at an annual time scale for all periods (Fig. S7 and Tables S1–S2). As for the distribution of NDVI trend, greening trend changed significantly from arid area to semi-humid area. The greening was rapid during the last decade with average rates of $0.83 \pm 4.04 \times 10^{-3}\ yr^{-1}$ in P2 and $5.33 \pm 10.49 \times 10^{-3}\ yr^{-1}$ in P3. The regions with significantly increased NDVI accounted for 35% of the total area ($P < 0.05$), and aggregate in the revegetation area (Figs. 1d and. S10). Evapotranspiration showed a decreasing trend throughout the LPC and in Rainfall zone I and II during 1982–2015, while displayed an increasing and fluctuating trend in Rainfall zone III (Fig. S8, Tables S1–S2). For precipitation, it decreased in the LPC and semi-humid area, but increased in arid and semi-arid area (Fig. S9, Tables S1–S2). The increasing trend of rainfall in the revegetated area was significantly much higher than that in the surrounding area ($P < 0.05$, Fig. S9). And the change trends of evapotranspiration and precipitation had no significance ($P > 0.05$, Fig. S10).

3.3. Relationship between NDVI, evapotranspiration and precipitation and SM at spatio-temporal scale

Given that the partial correlation of SM with NDVI was significantly higher than that with evapotranspiration and precipitation, NDVI was considered as the most important factor in SM dynamics from 1982 to 2015. Less than 92% (30%, $P < 0.05$) of 1029 pixels showed a positive correlation and 78% (27%, $P < 0.05$) of pixels show a negative correlation between NDVI with SM (Table S3). For evapotranspiration, less than 8% of the pixels exhibited significantly positive correlation and 7% of pixels exhibit significantly negative correlation with SM. Precipitation showed a significantly positive effect on SM in relatively dry region, with less than 76% (24%, $P < 0.05$) of pixels exhibiting positive correlation with SM. These results exhibited that satellite-based SM was more sensitive to NDVI than to evapotranspiration and precipitation, especially in wet region during dry season and dry region during wet season (Fig. S12). We further explored the dominant driver by decomposing of regression coefficients when regressing SM in both root-zone and surface soil against NDVI, evapotranspiration, and precipitation (Fig. 4). The dominant driver to SM variation varies widely across the LPC. Vegetation activity was the dominant driver in root-zone SM for about 49% of the area and in surface SM for about 46% of the area, while evapotranspiration and precipitation spread over Mu Us Desert, central LPC, Southwest LPC, and eastern LPC (Fig. 4). SM variation over the revegetated areas of LPC is dominantly drived by vegetation activity, suggesting GGP is driving the SM variability, especially for root-zone SM.

Considering the important role of NDVI in SM dynamics, the pixels were classified according to the NDVI value (> 0.1, defined as vegetated areas) with an interval of 0.05. The results showed that the effects of the driving factors for SM dynamics under different vegetation covers are strongly dependent on season and local rainfall (Fig. 5). NDVI had a moderately and significantly positive effect on root-zone SM when NDVI ≤ 0.275 in the LPC or semi-arid area and when NDVI was close to 0.125 in arid area ($P < 0.20$, Fig. 5a–c). NDVI had a strongly negative effect on SM in the area with a relatively sparse vegetation (NDVI $\leq$ 0.325) or dense vegetation (NDVI > 0.525) in Rainfall zone III, especially for surface SM (Fig. 5d). Precipitation had a moderately and significantly positive and dominant effect on SM when NDVI ≤ 0.15 for arid area and the whole plateau and when NDVI ≤ 0.2 for semi-arid area ($P < 0.20$). In addition, precipitation had a greater impact on SM in surface soil than in root-zone soil. In the semi-arid area with NDVI > 0.2, a moderately significant effect of evapotranspiration on SM was found ($P < 0.20$).

Then, the pixels were classified as cropland (C), forestland (F), grassland (G), and bareland (B) to identify the dominant driving factors for SM dynamics under different land use types (Table 1). In root-zone soil, the SM under all land use types was mainly controlled by NDVI, with 74% (25%, C), 55% (9%, F), 87% (28%, G), and 69% (12%, B) of pixels exhibiting positive partial coefficients in arid and semi-arid areas ($P < 0.05$, land use type), respectively. NDVI mainly had a negative effect on SM in wet region, with 70% (8%), 67% (6%) and 78% (9%) pixels of cropland, forestland and grassland having negative partial correlation ($P < 0.05$), respectively. NDVI, evapotranspiration and precipitation showed stronger effects on surface SM than on root-zone SM. For precipitation in bareland, 82% (2%) and 82% (4%) pixels of the entire area and arid area exhibited positive partial coefficients ($P < 0.05$), respectively. These results indicated that precipitation has more significant effects on SM in surface soil, non-vegetated areas, sparsely vegetated area or dry region ($P < 0.05$). In general, annual SM was much more strongly correlated with NDVI in both root-zone and surface soil than evapotranspiration and precipitation in semi-humid area, but the effect of NDVI became more coupled with that of evapotranspiration or precipitation in the arid and semi-arid area under all land use types.

3.4. Contributions of NDVI, evapotranspiration and precipitation to SM

We compared the relative importance of vegetation activity of grassland and woodland, evapotranspiration, and precipitation in SM dynamics in each stage of GGP (Fig. 6), and found that their contributions to SM dynamics are significantly different. Besides, the vegetation activities of grassland and woodland revegetated areas exhibited distinct contributions to SM dynamics.

Before the implementation of GGP, the SM was directly controlled by precipitation (0.491), evapotranspiration (–0.196) and NDVI (0.186) in surface soil. The relatively low vegetation transpiration effect in cropland (0.086) leaded to a less reduction of SM, especially for surface soil. However, evapotranspiration had a significant and indirect contribution to SM through promoting rainfall ($P < 0.05$, Fig. 6). At the beginning of large-scale GGP implementation, there were anomalous effects of evapotranspiration, precipitation and NDVI on SM in woodland revegetated areas. For example, evapotranspiration (0.542) positively contributes while precipitation (–0.413) negatively contributes to SM. The grassland revegetated areas were mainly located in rain-fed arid and semi-arid regions. Hence, the contribution of rainfall was still significantly positive, with the values of 0.515 and 0.241 for root-zone and surface SM, respectively ($P < 0.05$). In the early stage of GGP, the negative contribution of vegetation transpiration to SM was peaking, with the values of –0.482 and –0.569 in root-zone and surface SM, which was greater in woodland than in grassland. After the implementation of GGP, the contributions of the driving factors for SM dynamics followed the order of precipitation > NDVI > evapotranspiration in revegetated grassland at all stages of GGP and evapotranspiration > precipitation > NDVI in revegetated woodland especially during the early stage. Moreover, the vegetation activity first affected the rainfall occurrence, and then did the SM.

4. Discussion

There had an obvious and downward gradient in annual SM from northwestern to southeastern LPC, and Mu Us desert is the most severe arid area in the LPC (Fig. 2), which was consistent with the result of Wang et al. (2011) who studied the spatial distribution of SM throughout the LPC with a large amount of sample data. According to the method in the previous study (Feng et al., 2017), we found that the relationship between GLEAM SM and MODIS LAI/LST was consistent with those between in situ SM and MODIS LAI/LST (Fig. S1). These results indicated that GLEAM SM is also suitable for evaluating the spatio-temporal variations of SM in the LPC just as JAXA SM.

At the 34-year time scale, NDVI played a key role in the vertical and horizontal distribution of SM. At the beginning of GGP implementation, the intense human disturbance such as irrigation in woodland revegetated areas leads to anomalous effects of evapotranspiration, precipitation and NDVI on SM (Zhou et al., 2009). The indirect

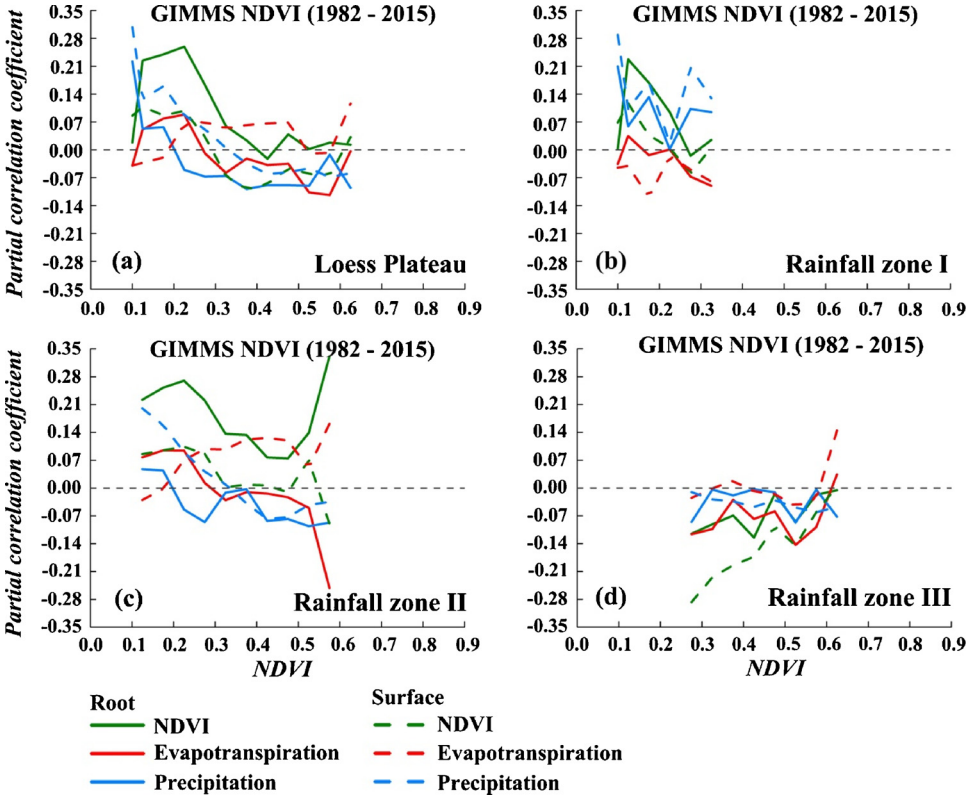

Fig. 5. Partial correlation coefficients between annual SM and NDVI (green), evapotranspiration (red), and precipitation (blue) along the NDVI gradient during the period of 1982–2015. The NDVI gradient is constructed using different classes of NDVI with an interval of 0.05. SM and NDVI represent soil moisture and normalized difference vegetation index, respectively. (For interpretation of the references to colour in this figure legend, the reader is referred to the web version of this article.)

Table 1
The area percentages of positive/negative partial correlation coefficient (statistically significant at $P < 0.1$) between soil moisture and NDVI, E, and Pr during 1982–2015 for each land use type.

Land use	Factors	Sign	Percentage (%)							
			SMroot				SMsurf			
			All	I	II	III	All	I	II	III
C	NDVI	+ [a]	74 (**25**)	54 (**19**)	95 (**35**)	30 (**3**)	53 (**6**)	62 (**8**)	66 (**7**)	20 (**3**)
		– [a]	26 (**3**)	46 (0)	5 (0)	70 (**8**)	47 (**9**)	38 (**4**)	34 (**1**)	80 (**29**)
	E	+ [a]	53 (**3**)	46 (0)	67 (**4**)	23 (0)	63 (**9**)	46 (0)	75 (**12**)	39 (**2**)
		– [a]	47 (**1**)	54 (0)	33 (0)	77 (**3**)	37 (**1**)	54 (**4**)	25 (0)	61 (0)
	Pr	+ [a]	26 (**1**)	54 (**4**)	32 (0)	6 (0)	60 (**6**)	69 (**8**)	67 (**8**)	42 (0)
		– [a]	74 (0)	46 (0)	68 (0)	94 (0)	40 (0)	31 (0)	33 (0)	58 (0)
F	NDVI	+ [a]	55 (**9**)	0 (0)	76 (**18**)	33 (0)	46 (**6**)	0 (0)	62 (**11**)	29 (0)
		– [a]	45 (**3**)	0 (0)	24 (0)	67 (**6**)	54 (**6**)	0 (0)	38 (**1**)	71 (**11**)
	E	+ [a]	27 (**1**)	0 (0)	25 (**1**)	28 (0)	50 (**6**)	0 (0)	61 (**10**)	40 (**3**)
		– [a]	73 (**8**)	0 (0)	75 (**10**)	72 (**6**)	50 (0)	0 (0)	39 (0)	60 (0)
	Pr	+ [a]	12 (0)	0 (0)	10 (0)	14 (0)	18 (**1**)	0 (0)	14 (**1**)	22 (0)
		– [a]	88 (0)	0 (0)	90 (0)	86 (0)	82 (0)	0 (0)	86 (0)	78 (0)
G	NDVI	+ [a]	87 (**28**)	86 (**33**)	92 (**29**)	22 (0)	67 (**9**)	71 (**26**)	71 (**7**)	13 (0)
		– [a]	13 (**1**)	14 (0)	8 (0)	78 (**9**)	33 (**3**)	29 (**2**)	29 (**1**)	87 (0)
	E	+ [a]	61 (**6**)	52 (**2**)	65 (**8**)	35 (0)	53 (**5**)	34 (0)	59 (**7**)	30 (0)
		– [a]	39 (**1**)	48 (**4**)	35 (0)	65 (0)	47 (**2**)	66 (**7**)	41 (**1**)	70 (0)
	Pr	+ [a]	45 (0)	78 (0)	42 (0)	4 (0)	61 (**11**)	69 (**16**)	63 (**11**)	17 (0)
		– [a]	55 (0)	22 (0)	58 (0)	96 (0)	39 (0)	31 (0)	37 (0)	83 (0)
B	NDVI	+ [a]	69 (**12**)	61 (**11**)	85 (**15**)	0 (0)	57 (**8**)	57 (**11**)	60 (**5**)	0 (0)
		– [a]	31 (0)	39 (0)	15 (0)	0 (0)	43 (**6**)	43 (**4**)	40 (**5**)	0 (0)
	E	+ [a]	47 (0)	43 (0)	55 (0)	0 (0)	39 (0)	43 (0)	30 (0)	0 (0)
		– [a]	53 (0)	57 (0)	45 (0)	0 (0)	61 (0)	57 (**14**)	70 (0)	0 (0)
	Pr	+ [a]	82 (**2**)	82 (**4**)	85 (0)	0 (0)	88 (**33**)	82 (**50**)	100 (**10**)	0 (0)
		– [a]	18 (0)	18 (0)	15 (0)	0 (0)	12 (0)	18(0)	0 (0)	0 (0)

SMroot: soil moisture in root-zone soil; SMsurf: soil moisture in surface soil; I: Rainfall zone I (< 250 mm); II: Rainfall zone II (250–500 mm); III: Rainfall zone III (> 500 mm); C: Cropland; F: Forestland; G: Grassland; B: Bareland; NDVI: normalized difference vegetation index; E: evapotranspiration; Pr: precipitation; plus sign (+): positive percentages; minus sign (–): negative percentages; [a] statistically significant at $P < 0.1$.

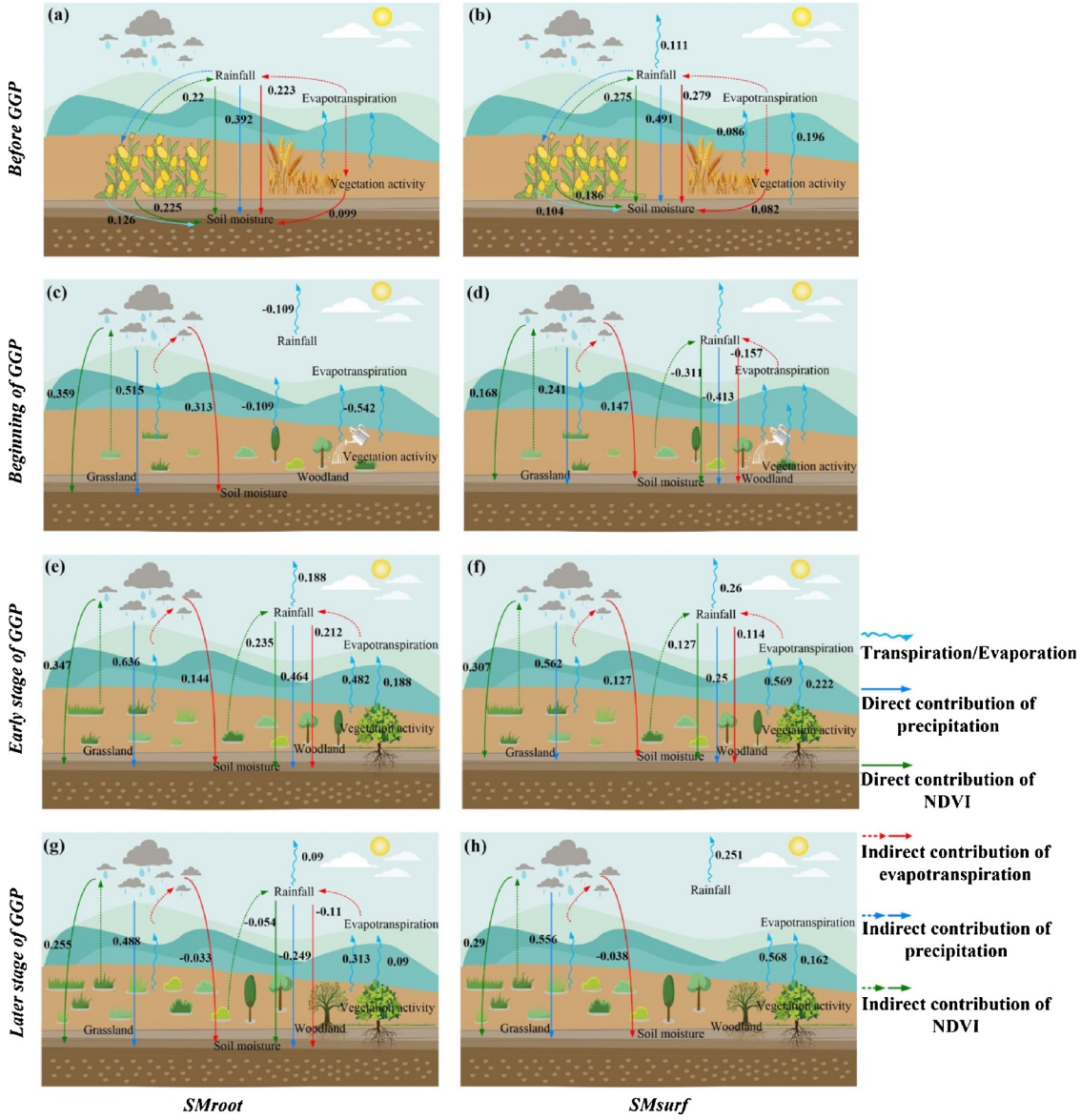

Fig. 6. Path analysis showing the direct/indirect contributions of NDVI, evapotranspiration and precipitation on SM in the afforested area during four periods: 1982–1998 (before GGP), 1999 (beginning of GGP), 2000–2007 (early stage of GGP) and 2008–2015 (later stage of GGP). $P < 0.01$, statistically significant. The contributions are estimated in root-zone (a, c, e and g) and surface (b, d, f and h) soil, respectively. GGP, SM, and NDVI represent "Grain for Green" project, soil moisture, and normalized difference vegetation index, respectively.

contributions of these driving factors were opposite to those in the stages or areas with limited human disturbance. Some studies have shown that the vegetation activity in the LPC increases at the cost of soil water overconsumption (Zhang et al., 2012). However, our study demonstrated that the soil water consumption in response to vegetation activity heavily depended on the local precipitation, vegetation type, vegetation density and human activity. Soil water overconsumption is mainly found in the areas with MAP > 450 mm (Figs. 1 and 3). The rainfall band with MAP = 450 mm was the boundary of forestland and grassland. A large area of forest in semi-humid area decreases SM by increasing leaf interception and root water uptake (Wang et al., 2010). The grassland retained more precipitation in the soil due to the shallow root distribution, low water uptake capacity (Wang et al., 2012), high percolation, and low evapotranspiration (Bellot et al., 1999). In addition, Adair et al. (2011) proposed that CO_2 induced the declines of stomatal conductance and plant water use in grassland and thus increases the SM. Zavaleta et al. (2003) suggested that water-limited ecosystems would increase spring SM content by 5–10% because of the feedback of plants to the global warming conditions.

Feng et al. (2017) showed that the precipitation has a significantly positive effect on SM. In fact, at the 34-year time scale, the significantly positive effect of precipitation on SM was only found in bareland and sparse vegetation area. Altogether, vegetation activity had a certain effect on the occurrence of rainfall, and then affected on the SM. Forzieri et al. (2017) reported that an increase in leaf area index contributes to the warming of boreal zones through reducing the land surface albedo and the evaporation-driven cooling in arid areas. The increasing cloudiness before and after raining may negatively affect the derivation of SM and NDVI data because of the effects of cloud and aerosol contamination on surface reflectance and net radiation, which may lead to an imprecise evaluation of the SM and NDVI trend (Nicolai-Shaw et al., 2017). Signal contamination or saturation problems may influence NDVI under high rainfall or biomass circumstances (Wang et al., 2017b). Furthermore, satellite-based SM was not synchronous with the rainfall due to the instantaneity of satellite data (Kustas et al., 1990). Therefore, it seems a paradox that precipitation has no

significant effect on SM for all land use types except for bareland, however, the reasonability has been verified by the above-mentioned facts.

Our results of spatio-temporal analysis highlight the necessity to pay due attention to the appropriate layout of vegetation density, growth age and species composition, particularly the planting in drylands. Based on abovementioned results, we performed a preliminary assessment of GGP effect on SM in the LPC (Fig. S13). Interestingly, it was potentially beneficial to restore vegetation with the aim to further enhancing the ecosystem services in drylands with sparse or excessively sparse vegetation cover, especially in desert (Fig. S13c), until the vegetation fraction (Fv) (SI, Section 1.3) reached the optimal vegetation cover, namely 1.4%–3.7% and 3.8%–7.2%, respectively. Those indicated that sand-fixing vegetation plays a significant role in restoring ecological functions. In these areas, an increasing vegetation activity contributes to a strongest positive effect on soil water retention compared to other areas. Li (2011) found that SM in the grassland was significantly higher than SM in the bare land except for the SM in 10–20 cm based on long-term monitoring data in Inner Mongolia. It has proved that the grassland conserves more water than the bare land. Its intrinsic mechanism is the efficient use and accumulation of water (Schlesinger and Pilmanis, 1998). However, vegetation cover increases at the cost of overconsumption of soil water in semi-humid area, while the effect was not significant when the Fv is 33.3%–53.4% (appropriate zone just for semi-humid area in Fig. S13 b). In brief, vegetation should be maintained rather than further expanded in entire semi-humid area and arid or semi-arid areas with excessively dense, dense or appropriate vegetation cover.

5. Conclusions

An integrated method based on a variety of satellite data products had proposed to provide a systematic and quantitative assessment of the revegetation drivers in spatio-temporal dynamics of SM. And this method could be applied to other places without a SM monitoring network. This study confirmed the availability of GLEAM SM in evaluating the spatio-temporal variations of SM in the LPC. At the 34-year time scale, revegetation played a dominant role in SM dynamics in vegetated areas, and turned the wet region (MAP $>$ 450 mm) to be dry and dry region to be wet, which was attributable to the differences in vegetation structure, density, growth age, and species. The significantly positive effect of precipitation on SM was only found in bareland and sparsely vegetated area. Evapotranspiration had an important effect on SM in bareland, sparsely vegetated area or densely vegetated area. At the spatial scale, the driving effect of vegetation cover on SM dynamics was relatively weak due to the more significant role of evapotranspiration and precipitation. Evapotranspiration played a dominant role in SM dynamic in revegetated woodland, especially in the early stage of GGP (From 2000–2010), while precipitation and vegetation cover had much greater contributions to SM than evapotranspiration in revegetated grassland. Therefore, our findings highlight the importance of spatial analysis to investigate the interactions between SM and vegetation activity and alert the excessive reliance on afforestation. Our study suggests that vegetation should not be further expanded in semi-humid areas, but should be further restored in arid and semi-arid areas with sparse or excessively sparse vegetation cover (especially in desert).

Acknowledgments

This work was supported by National Natural Science Foundation of China (Nos. 41330852 and 41425006) and the National Key Basic Research Program of China (No. 2015CB150504). We are also grateful to Mr. Zuoxiong Liu and Dr. Dong-Gill Kim for improving the English language.

Appendix A. Supplementary data

Supplementary material related to this article can be found, in the online version, at doi:https://doi.org/10.1016/j.agee.2018.10.006.

References

Adair, E.C., Reich, P.B., Trost, J.J., Hobbie, S.E., 2011. Elevated CO_2 stimulates grassland soil respiration by increasing carbon inputs rather than by enhancing soil moisture. Glob. Change Biol. 17 (12), 3546–3563.
Bellot, J., Sanchez, J.R., Chirino, E., Hernandez, N., Abdelli, F., Martinez, J.M., 1999. Effect of different vegetation type cover on the soil water balance in semi-arid areas of South Eastern Spain. Phys. Chem. Earth Part B 24 (4), 353–357.
Chen, H.S., Shao, M.A., Li, Y.Y., 2008. Soil desiccation in the Loess Plateau of China. Geoderma 143 (1), 91–100.
Chen, J., Chen, J., Liao, A.P., Cao, X., Chen, L.J., Chen, X.H., He, C.Y., Han, G., Peng, S., Lu, M., 2015a. Global land cover mapping at 30m resolution: a POK-based operational approach. ISPRS J. Photogramm. Remote Sens. 103, 7–27.
Chen, Y.P., Wang, K.B., Lin, Y.S., Shi, W.Y., Song, Y., He, X.H., 2015b. Balancing green and grain trade. Nat. Geosci. 8 (10), 739–741.
Deng, L., Liu, S.G., Kim, G.D., Peng, C.H., Sweeney, S., Shangguan, Z.P., 2017. Past and future carbon sequestration benefits of China's grain for green program. Glob. Environ. Change 47, 13–20.
Deng, L., Shangguang, Z.P., Li, R., 2012. Effects of the grain-for-green programme on soil erosion in China. Int. J. Sediment Res. 27 (1), 120–127.
Deng, L., Yan, W.M., Zhang, Y.W., Shangguan, Z.P., 2016. Severe depletion of soil moisture following land-use changes for ecological restoration: evidence from northern China. For. Ecol. Manage. 366, 1–10.
Durocher, M.G., 1990. Monitoring spatial variability of forest interception. Hydrol. Processes 4 (3), 215–229.
Feng, X.M., Fu, B.J., Piao, S.L., Wang, S., Ciais, P., Zeng, Z.Z., Lü, Y.H., Zeng, Y., Li, Y., Jiang, X.H., 2016. Revegetation in China's Loess Plateau is approaching sustainable water resource limits. Nat. Clim. Change 6 (11), 1019–1022.
Feng, X.M., Li, J.X., Cheng, W., Fu, B.J., Wang, Y.Q., Lü, Y.H., Shao, M.A., 2017. Evaluation of AMSR-E retrieval by detecting soil moisture decrease following massive dryland re-vegetation in the Loess Plateau, China. Remote Sens. Environ. 196, 253–264.
Forzieri, G., Alkama, R., Miralles, D.G., Cescatti, A., 2017. Satellites reveal contrasting responses of regional climate to the widespread greening of earth. Science 356 (6343), 1180–1184.
Fu, B.J., 1989. Soil erosion and its control in the loess plateau of China. Soil Use Manage. 5 (2), 76–82.
Gromping, U., 2006. Relative importance for linear regression in R: the package relaimpo. J. Stat. Softw. 17 (1), 925–933.
Huang, J.P., Ji, M.X., Xie, Y.K., Wang, S.S., He, Y.L., Ran, J.J., 2016. Global semi-arid climate change over last 60 years. Clim. Dyn. 46 (3), 1131–1150.
Jasechko, S., Sharp, Z.D., Gibson, J.J., Birks, S.J., Yi, Y., Fawcett, P.J., 2013. Terrestrial water fluxes dominated by transpiration. Nature 496 (7445), 347–350.
Jiao, Q., Li, R., Wang, F., Mu, X.M., Li, P.F., An, C.C., 2016. Impacts of re-vegetation on surface soil moisture over the Chinese Loess Plateau based on remote sensing datasets. Remote Sens. 8 (2), 156.
Kustas, W.P., Moran, M.S., Jackson, R.D., Gay, L.W., Duell, L.F.W., Kunkel, K.E., Matthias, A.D., 1990. Instantaneous and daily values of the surface energy balance over agricultural fields using remote sensing and a reference field in an arid environment. Remote Sens. Environ. 32 (2), 125–141.
Lawrence, D., Vandecar, K., 2014. Effects of tropical deforestation on climate and agriculture. Nat. Clim. Change 5 (1), 27–36.
Li, X.Y., 2011. Mechanism of coupling, response and adaptation between soil, vegetation and hydrology in arid and semiarid regions. Sci. Sin. Terrae 41 (12), 1721–1730 (in Chinese).
Li, Y.S., Huang, M.B., 2008. Pasture yield and soil water depletion of continuous growing alfalfa in the Loess Plateau of China. Agric. Ecosyst. Environ. 124 (1), 24–32.
Li, Y.Y., Shao, M.A., 2006. Change of soil physical properties under long-term natural vegetation restoration in the Loess Plateau of China. J. Arid Environ. 64 (1), 77–96.
Llorens, P., Domingo, F., 2007. Rainfall partitioning by vegetation under Mediterranean conditions. A review of studies in Europe. J. Hydrol. 335 (1), 37–54.
Manoli, G., Domec, J.C., Novick, K., Oishi, A.C., Noormets, A., Marani, M., Katul, G., 2016. Soil-plant-atmosphere conditions regulating convective cloud formation above southeastern US pine plantations. Glob. Change Biol. 22 (6), 2238–2254.
Mao, D.H., Wang, Z.M., Luo, L., Ren, C.Y., 2012. Integrating AVHRR and MODIS data to monitor NDVI changes and their relationships with climatic parameters in Northeast China. Int. J. Appl. Earth Obs. Geoinf. 18 (Supplement C), 528–536.
Martens, B., Miralles, D., Lievens, H., Fernández-Prieto, D., Verhoest, N.E.C., 2016. Improving terrestrial evaporation estimates over continental Australia through assimilation of SMOS soil moisture. Int. J. Appl. Earth Obs. Geoinf. 48, 146–162.
Martens, B., Gonzalez Miralles, D., Lievens, H., van der Schalie, R., de Jeu, R.A., Fernández-Prieto, D., Beck, H.E., Dorigo, W., Verhoest, N., 2017. GLEAM v3: satellite-based land evaporation and root-zone soil moisture. Geosci. Model Dev. 10 (5), 1903–1925.
McColl, K.A., Alemohammad, S.H., Akbar, R., Konings, A.G., Yueh, S., Entekhabi, D., 2017. The global distribution and dynamics of surface soil moisture. Nat. Geosci. 10 (2), 100–104.
Miralles, D.G., De Jeu, R.A.M., Gash, J.H.C., Holmes, T.R.H., Dolman, A.J., 2011. Magnitude and variability of land evaporation and its components at the global scale.

Hydrol. Earth Syst. Sci. 15 (3), 967–981.
Nicolai-Shaw, N., Zscheischler, J., Hirschi, M., Gudmundsson, L., Seneviratne, S.I., 2017. A drought event composite analysis using satellite remote-sensing based soil moisture. Remote Sens. Environ. 203 (Supplement C), 216–225.
Ortiz, R., Sayre, K.D., Govaerts, B., Gupta, R., Subbarao, G.V., Ban, T., Hodson, D., Dixon, J.A., Ortiz-Monasterio, J.I., Reynolds, M., 2008. Climate change: can wheat beat the heat? Agric. Ecosyst. Environ. 126 (1–2), 46–58.
Park, S., Im, J., Park, S., Rhee, J., 2017. Drought monitoring using high resolution soil moisture through multi-sensor satellite data fusion over the Korean peninsula. Agric. For. Meteorol. 237–238, 257–269.
Peng, J., Liu, Y., Liu, Z., Yang, Y., 2017. Mapping spatial non-stationarity of human-natural factors associated with agricultural landscape multifunctionality in Beijing–Tianjin–Hebei region, China. Agric. Ecosyst. Environ. 246, 221–233.
Piao, S.L., Ciais, P., Friedlingstein, P., Peylin, P., Reichstein, M., Luyssaert, S., Margolis, H.A., Fang, J.Y., Barr, A., Chen, A.P., 2008. Net carbon dioxide losses of northern ecosystems in response to autumn warming. Nature 451 (7174), 49–52.
Piao, S.L., Fang, J.Y., Zhou, L.M., Ciais, P., Zhu, B., 2006. Variations in satellite-derived phenology in China's temperate vegetation. Glob. Change Biol. 12 (4), 672–685.
Reynolds, J.F., Smith, D.M.S., Lambin, E.F., Turner II., B.L., Mortimore, M., Batterbury, S.P., Downing, T.E., Dowlatabadi, H., Fernandez, R.J., Herrick, J.E., Huber-Sannwald, E., Jiang, H., Leemans, R., Lynam, T., Maestre, F.T., Ayarza, M., Walker, B., 2007. Global desertification: building a science for dryland development. Science 316 (5826), 847–851.
Schlaepfer, D.R., Bradford, J.B., Lauenroth, W.K., Munson, S.M., Tietjen, B., Hall, S.A., Wilson, S.D., Duniway, M.C., Jia, G., Pyke, D.A., Lkhagva, A., Jamiyansharav, K., 2017. Climate change reduces extent of temperate drylands and intensifies drought in deep soils. Nat. Commun. 8, 14196.
Schlesinger, W.H., Pilmanis, A.M., 1998. Plant-soil interactions in deserts. Biogeochemistry 42 (1/2), 169–187.
Van Loon, A.F., Gleeson, T., Clark, J., Van Dijk, A.I.J.M., Stahl, K., Hannaford, J., Di Baldassarre, G., Teuling, A.J., Tallaksen, L.M., Uijlenhoet, R., Hannah, D.M., Sheffield, J., Svoboda, M., Verbeiren, B., Wagener, T., Rangecroft, S., Wanders, N., Van Lanen, H.A.J., 2016. Drought in the anthropocene. Nat. Geosci. 9 (2), 89–91.
Velicer, W.F., 1976. Determining the number of components from the matrix of partial correlations. Psychometrika 41 (3), 321–327.
Wang, J.R., 1985. Effect of vegetation on soil moisture sensing observed from orbiting microwave radiometers. Remote Sens. Environ. 17 (2), 141–151.
Wang, X.L., Sun, G.J., Jia, Y., Li, F.M., Xu, J.Z., 2008. Crop yield and soil water restoration on 9-year-old alfalfa pasture in the semiarid Loess Plateau of China. Agric. Water Manage. 95 (3), 190–198.
Wang, Y.Q., Shao, M.A., Shao, H.B., 2010. A preliminary investigation of the dynamic characteristics of dried soil layers on the Loess Plateau of China. J. Hydrol. 381 (1), 9–17.
Wang, Y.Q., Shao, M.A., Zhu, Y.J., Liu, Z.P., 2011. Impacts of land use and plant characteristics on dried soil layers in different climatic regions on the Loess Plateau of China. Agric. Forest Meteorol. 151, 437–448.
Wang, S., Fu, B.J., Gao, G.Y., Yao, X.L., Zhou, J., 2012. Soil moisture and evapotranspiration of different land cover types in the Loess Plateau, China. Hydrol. Earth Syst. Sci. 16 (8), 2883–2892.
Wang, X.Y., Wang, T., Guo, H., Liu, D., Zhao, Y.T., Zhang, T.T., Liu, Q., Piao, S.L., 2017a. Disentangling the mechanisms behind winter snow impact on vegetation activity in northern ecosystems. Glob. Change Biol. 24 (4), 1651–1662.
Wang, X.Y., Wang, T., Liu, D., Guo, H., Huang, H.B., Zhao, Y.T., 2017b. Moisture-induced greening of the South Asia over the past three decades. Glob. Change Biol. 23 (11), 4995–5005.
Xin, Z.B., Yu, X.X., Li, Q.Y., Lu, X.X., 2011. Spatiotemporal variation in rainfall erosivity on the Chinese loess plateau during the period 1956–2008. Reg. Environ. Change 11 (1), 149–159.
Yang, L., Wei, W., Chen, L.D., Chen, W.L., Wang, J.L., 2014. Response of temporal variation of soil moisture to vegetation restoration in semi-arid Loess Plateau, China. Catena 115, 123–133.
Yang, Y., Dou, Y.X., Liu, D., An, S.S., 2017. Spatial pattern and heterogeneity of soil moisture along a transect in a small catchment on the Loess Plateau. J. Hydrol. 550, 466–477.
Yuan, Z., Yu, K., Guan, X., Fang, C., Li, M., Shi, X., Li, F., 2016. Medicago sativa improves soil carbon sequestration following revegetation of degraded arable land in a semi-arid environment on the Loess Plateau, China. Agric. Ecosyst. Environ. 232, 93–100.
Zavaleta, E.S., Thomas, B.D., Chiariello, N.R., Asner, G.P., Shaw, M.R., Field, C.B., 2003. Plants reverse warming effect on ecosystem water balance. Proc. Natl. Acad. Sci. U. S. A. 100 (17), 9892–9893.
Zhang, B.Q., Wu, P.T., Zhao, X.N., Wang, Y.B., Wang, J.W., Shi, Y.G., 2012. Drought variation trends in different subregions of the Chinese Loess Plateau over the past four decades. Agric. Water Manage. 115, 167–177.
Zhang, T.T., Wen, J., Su, Z.B., Velde, Rvd., Timmermans, J., Liu, R., Liu, Y.Y., Li, Z.C., 2009. Soil moisture mapping over the Chinese Loess Plateau using ENVISAT/ASAR data. Adv. Space Res. 43 (7), 1111–1117.
Zhao, B.H., Li, Z.B., Li, P., Xu, G.C., Gao, H.D., Cheng, Y.T., Chang, E.H., Yuan, S.L., Zhang, Y., Feng, Z.H., 2017. Spatial distribution of soil organic carbon and its influencing factors under the condition of ecological construction in a hilly-gully watershed of the Loess Plateau, China. Geoderma 296, 10–17.
Zhou, H.J., Van Rompaey, A., Wang, J.A., 2009. Detecting the impact of the "Grain for Green" program on the mean annual vegetation cover in the Shaanxi province, China using SPOT-VGT NDVI data. Land Use Policy 26 (4), 954–960.
Zhou, D., Zhao, S., Zhu, C., 2012. The Grain for Green project induced land cover change in the Loess Plateau: a case study with Ansai County, Shanxi Province, China. Ecol. Indic. 23, 88–94.